Experimental and theoretical analysis of magnetic moment enhancement in oxygen-deficient EuO

M. Barbagallo,[1,*] N. D. M. Hine,[1,2] J. F. K. Cooper,[1] N.-J. Steinke,[1] A. Ionescu,[1] C. H. W. Barnes,[1,†] C. J. Kinane,[3] R. M. Dalgliesh,[3] T. R. Charlton,[3] and S. Langridge[3]

[1]*Cavendish Laboratory, Physics Department, University of Cambridge, Cambridge CB3 0HE, United Kingdom*

[2]*Thomas Young Centre, Department of Materials and Department of Physics, Imperial College, London WC1H 0AH, United Kingdom*

[3]*ISIS, Harwell Science and Innovation Campus, STFC, Oxon OX11 0QH, United Kingdom*

(Received 22 March 2010; revised manuscript received 8 May 2010; published 29 June 2010)

We have carried out both experimental and theoretical studies of the magnetic properties of thin films of oxygen-deficient EuO. Accurate control of the oxygen vacancy concentration in these films was achieved by sputter codeposition of Eu and Eu_2O_3. The films were characterized by superconducting quantum interference device, x-ray reflectometry and polarized neutron reflectometry and the magnetic moment was found to increase monotonically with oxygen vacancy concentration. The electronic structure of EuO_{1-x} was calculated using density-functional theory (DFT+U). In agreement with previous studies, these calculations show that oxygen vacancies act as n-type dopants in EuO and that the excess electrons preferentially populate the majority spin branch of the spin-polarized conduction band. The observed increase in the magnetic moment originating from these excess electrons was accurately determined experimentally and found to be in good agreement with our quantitative predictions.

DOI: 10.1103/PhysRevB.81.235216 PACS number(s): 75.70.−i, 75.50.Pp, 75.47.Lx, 71.15.Mb

I. INTRODUCTION

In 1999 DiVincenzo proposed the use of thin-film EuO as a spin-dependent tunnel barrier to enable single-shot measurement of spin qubits in Si/Ge or GaAs based quantum processors.[1,2] At the time, it was not known experimentally whether thin-film EuO would be compatible with the growth of Si or GaAs and whether its conductivity could be matched with these materials to enable it to operate as an efficient spin filter.[1] Subsequently the growth and spin-injection properties of thin-film EuO were shown to be compatible with Si, preserving a very high polarization, above 90% both for epitaxial[3] and nonepitaxial[4] thin films. The conductivity was matched with Si by introducing excess electrons into the conduction band of EuO by doping either with La (Ref. 3) or oxygen vacancies.[4] However a question still remained as to what effect, quantitatively, the excess electron concentration from the oxygen vacancies would have on the magnetic interactions in thin-film EuO and therefore the magnetic moment of this material, and how the polarization of the conduction band would be affected by varying the degree of nonstoichiometry.

In this paper we make an accurate analysis of the oxygen vacancy concentration, the magnetic moment, and the electronic band structure of oxygen-deficient EuO, therefore studying the interaction between these factors and consequently their effect on the polarization of the conduction band at the Fermi level. This study lets us draw a conclusive picture of the fundamental physics involved. Our density-functional theory (DFT) calculations, in agreement with previous studies,[5,6] show that the excess electrons which enable the conductivity matching also enhance the magnetic moment, by populating preferentially the majority spin branch of the spin-polarized conduction band. For higher oxygen vacancy concentrations the minority spin band is progressively lowered below the Fermi level, thereby decreasing the degree of polarization of the conduction band.

EuO is a ferromagnetic[7,8] semiconductor with a band gap of 1.12 eV and a conduction-band spin split by 0.6 eV (Refs. 9 and 10)—thin films of this material can therefore be very efficient spin filters.[11] Its Curie temperature T_c, for thin films, increases with doping from the intrinsic value of 70 K, up to 170 K reported for 4% Gd,[7,12,13] or by oxygen vacancies,[14–17] which are favored over interstitial Eu.[18] Stoichiometric EuO is an ideal Heisenberg ferromagnet with direct superexchange between the Eu 4f shells of nearest neighbors, however the excess electrons in the conduction band of doped EuO mediate an additional exchange, which is defined as indirect exchange by Mauger.[19] By varying the excess electron concentration it is possible to study how this additional exchange influences the Curie temperature and magnetic moment of thin films of EuO_{1-x}. Our study with varying oxygen vacancy concentration reproduces similar results for the Curie temperature to those previously found for EuO doped with Gd (Refs. 7, 12, and 13) and also determines quantitatively the effect on the magnetic moment.

This paper is organized as follows. In Sec. II we describe the sputtering growth process and the experimental details of the measurement techniques. Section III discusses the experimental results, in particular, the measurement of the magnetic moment and oxygen vacancy concentration of EuO_{1-x}. In Sec. IV we detail the electronic structure of EuO_{1-x}, studied by density-functional theory, and discuss how the spin polarization of the conduction band is influenced by the oxygen vacancy concentration.

II. EXPERIMENTAL METHODS

We deposited thin films of EuO_{1-x} by magnetron cosputtering using two targets: metallic Eu and ceramic Eu_2O_3. The oxygen-deficiency concentration was controlled by varying the relative growth rates from these two targets. Each sample contained about 20% of nonferromagnetic phases, e.g., Eu and Eu_2O_3. The base pressure in the chamber was 4

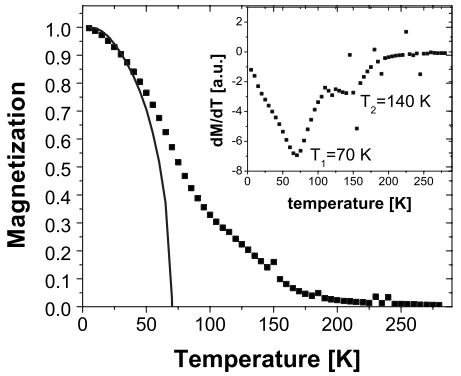

FIG. 1. Magnetization curve (normalized to unity) and first derivative (inset) for a 106 nm EuO_{1-x} film with $x_{PNR}=2.5\%$. The continuous line is the Brillouin $J=7/2$ function with $T_c=70$ K. Measured in a field of 1 T.

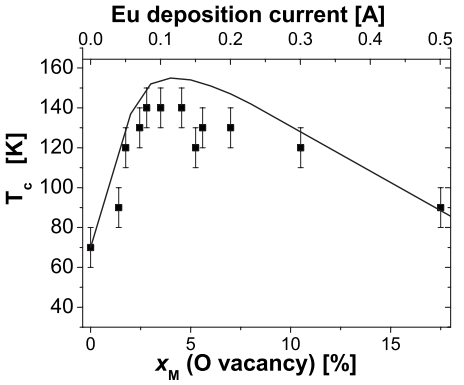

FIG. 2. T_c of 100-nm-thick EuO_{1-x} samples (data points) fitted with Mauger's model (line).

$\times 10^{-9}$ Torr and the Ar^+ pressure 2×10^{-3} Torr. The deposition rates were calibrated by x-ray reflectometry (XRR) and polarized neutron reflectometry (PNR) (Refs. 20–23) performed at 5 K on the CRISP station at ISIS with an in-plane field of 3 kOe.[24] PNR was also used to determine the magnetic moment of three samples with different oxygen vacancy concentrations x, which calculated from the PNR data[25] as detailed below, were $x_{PNR}=2.5\%$, 4.2%, and 9%. The deposition parameters and overall deposition rate for EuO_{1-x} for these samples were, respectively, as follows: Eu (0.10 A) and Eu_2O_3 (75 W), 3.5 nm/min; Eu (0.11 A) and Eu_2O_3 (75 W), 3.9 nm/min; and Eu (0.15 A) and Eu_2O_3 (50 W), 5.3 nm/min. All other samples were deposited by keeping the deposition rate for Eu_2O_3 constant (75 W). The magnetization curves of all samples were measured using a superconducting quantum interference device (SQUID) with an applied in-plane field of 1 T; the samples were saturated above 0.1 T. T_c was measured by linearly fitting, using the Curie-Weiss law, the data in the paramagnetic region. All samples (unless otherwise noted) were deposited at room temperature on (100) Si substrates with a Pt buffer layer and Pt capping layer both of 10 nm.

III. EXPERIMENTAL CHARACTERIZATION OF EuO_{1-x} THIN FILMS

A. SQUID measurements

A representative magnetization curve for EuO_{1-x} is shown in Fig. 1. The exchange interaction between Eu ions mediated by the conduction-band electrons causes a marked deviation from the Brillouin $J=7/2$ function.[3,14,26,27] As has been explained by Mauger and Godart,[7] the density of states of EuO_{1-x} changes with temperature because the spin splitting of the conduction band is a function of temperature; this mechanism produces two successive superimposed dome shapes in the magnetization curve with increasing temperature. These occur because EuO_{1-x}, in thin films, effectively behaves as if it has two Curie temperatures.[7,15,19,26,28,29] This can be seen in the inset of Fig. 1 which is the derivative of the magnetization with respect to temperature and has two minima, one at 70 K and the other at 140 K. In order to describe how T_c varies with the conduction-band electron concentration, we applied a model developed by Mauger for Gd doping;[7,27] we considered each oxygen vacancy to act like a Gd atom, donating one electron, the other electron is expected to remain localized.[7,8] By fitting the data to the model as shown in Fig. 2 we obtain a measurement of the oxygen vacancy concentration x which we denote as x_M, to distinguish it from that calculated by PNR, x_{PNR}. We extract from Mauger's model in Fig. 2 the expected values of x for the three samples measured by PNR (x_M). For the sample with $x_{PNR}=9\%$ the deposition rate for Eu_2O_3 was approximately half that of the other two samples. We therefore estimate x_M to be twice the value extracted from Fig. 2. This approximation arises because some of the deposited O comes from inside the chamber and not the Eu_2O_3 target. The values of x_M and x_{PNR} for the three samples will be compared in Table IV.

B. PNR measurements

We measured three samples by PNR: two samples with $x_{PNR}=2.5\%$ and 9% deposited on Si substrates whose natural oxide had been removed by HF etching, and one sample with $x_{PNR}=4.2\%$ deposited on a Pt buffer layer. The structure composition measured by PNR and XRR for each of the three PNR samples is shown in Table I. It can be seen that the films grown on etched Si have an increased roughness. The reflectivity data and fit to the standard model[25] are plotted in Fig. 3 for the three samples. From Table I it can be seen that the films thicknesses measured by XRR and PNR are in agreement to within a few Angstroms.

The other parameters of the PNR fit are the neutron-scattering length,[30] the number density, that is, the number of atoms per unit volume, the neutron absorption, and the magnetic moment of each layer. By fitting the PNR reflectivity data[25] as plotted in Fig. 3 we found that the best values for the effective scattering length and number density of EuO_{1-x} had a deviation from the theoretical stoichiometric ones. This was expected as the effective scattering length is the average of that of Eu and O, thus will change with the relative content of the two atoms, while the number density will depend on the degree of off stoichiometry, that is x, as well as the presence of extraneous nonmagnetic phases, that is Eu_2O_3

TABLE I. Thickness of samples with varying x_{PNR} (nanometer).

	Thickness		Roughness	
x_{PNR}=2.5%	PNR	XRR	PNR	XRR
Pt	13.1	12.2	1.8	1.1
EuO	7.0	8.7	2.3	1.1
Si(100)			1.1	0.6
x_{PNR}=9%				
Pt	11.2	10.7	1.6	1.5
EuO	11.5	10.8	2.1	1.3
Si(100)			1.2	0.6
x_{PNR}=4.2%				
Pt	12.2	11.8	1.3	0.7
EuO	10.9	11.2	0.9	0.8
Pt	11.7	12.3	1.4	1.2
Si(100)			0.3	0.3

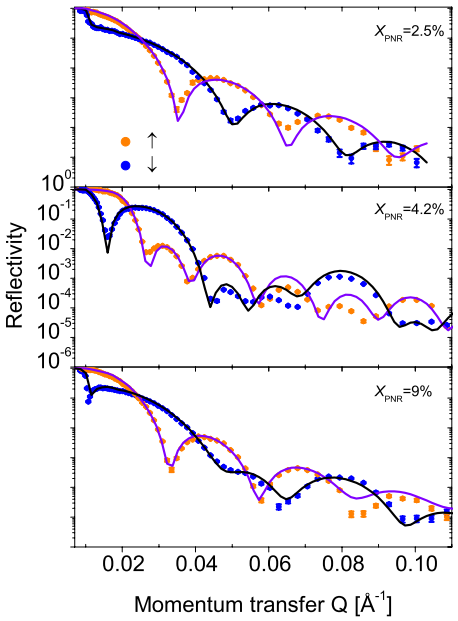

FIG. 3. (Color online) PNR data (data points) and fit (lines) for varying oxygen vacancy concentrations, x_{PNR}=2.5%, 4.2%, and 9%.

and Eu, that have a different number density. These parameters, listed in Table II, are instrumental in determining the exact magnetic moment of each sample. In fact, the PNR measurement gives the magnetic moment per atom of the magnetic layer, and it includes all nonmagnetic atoms as well. To extract the real magnetic moment per Eu atom of EuO_{1-x} we then have to exactly determine the number of magnetic atoms, that is we have to accurately measure x and the relative content of Eu_2O_3 and Eu, whose presence was detected also by x-ray diffraction (not shown). The effect of the nonmagnetic phases on the scattering length is measurable but less pronounced, as their b is relatively close to that of EuO; the effect on the absorption is minimal since their Eu atoms will also absorb neutrons. However, the effect on N is clearly detectable as the nonmagnetic phases have very different values for this parameter, compared to EuO. The values of N measured by PNR are all significantly reduced from the value for EuO and clearly indicate the presence of extraneous phases. These extraneous phases are modeled as clusters inside the film, hence a simple average for N and b is taken. The number density is also sensitive to x, therefore by finding the values for x as well as the fraction of Eu_2O_3 and Eu which reproduce the values of the scattering length, number density, and magnetic moment per atom measured by PNR we can accurately determine the number of magnetic Eu atoms. We found that the scattering length and number density were reproduced only by specific values for x and the fraction of nonmagnetic phases, which gave us confidence in the accuracy of the calculation. The fact that the values of x thus determined, x_{PNR}, are in very close agreement with those measured independently by using Mauger's model, x_M, gives strong support to the accuracy of the PNR parameters we calculated, listed in Table III. To distinguish the values of b and N obtained from the PNR fit from those we calculated starting from x and the nonmagnetic phases fractions to reproduce the former ones, we denote the former ones as PNR and the latter ones as C in Table III. The values of x_{PNR} and x_M can be compared in Table IV. The parameters of Table III have good consistency across the three samples, as the sample with x_{PNR}=2.5% has the lowest deposition rate for Eu and it has the highest fraction of Eu_2O_3, the lowest fraction of Eu and the lowest x; the sample with x_{PNR}=9% has the highest deposition rate for Eu, the highest fraction of Eu and the highest x. The values of magnetic moment per magnetic Eu atom thus calculated from the PNR data are all

TABLE II. Neutron-scattering length N and number density b for varying x_{PNR}.

	b (fm)	PNR fit b (fm)	PNR fit b (fm)	PNR fit b (fm)	N (10^{28}/m^3)	PNR fit N (10^{28}/m^3)	PNR fit N (10^{28}/m^3)	PNR fit N (10^{28}/m^3)
x_{PNR}		2.5%	4.2%	9%		2.5%	4.2%	9%
Pt	9.6	9.6	9.6	9.6	6.62	6.62	6.62	6.62
EuO	6.51	6.6	6.6	6.7	5.87	4.98	4.95	4.6
Eu	7.22				2.1			
Eu_2O_3	6.368				1.8			
Si	4.149				4.97			

TABLE III. Calculated fit of EuO_{1-x} parameters.

	b		*N*			
x_{PNR} (%)	PNR (fm)	C (fm)	PNR ($10^{28}/m^3$)	C ($10^{28}/m^3$)	Eu_2O_3 fraction (%)	Eu fraction (%)
2.5	6.6	6.57	4.98	4.98	14	7
4.2	6.6	6.62	4.95	4.95	10	11
9	6.7	6.69	4.6	4.61	12	16

increased relative to the theoretical value of $7\mu_B$ for stoichiometric EuO as seen in Table IV. In the literature values for the moment of EuO have been measured to be very close to[3,31] or below[4,14,32] $7\mu_B$ and in two cases above.[10,11] The wide range of values is probably attributable to the different growth conditions and uncertainty in the magnetometry technique used, which (with the exception of Ref. 3) relies on the precise measurement of the geometrical dimensions as well as the exact phase composition, of thin films, and can be more susceptible to imprecisions than PNR. An increase of the local exchange constant for EuO doped with Gd has been found previously via nuclear-magnetic resonance, although, contrary to our results, it was not monotonic.[33] We will discuss the values we measured for the magnetic moment and compare them with those predicted by DFT in Sec. V.

IV. ELECTRONIC-STRUCTURE CALCULATIONS

To determine the electronic structure of EuO_{1-x} and provide context for the experimental findings, plane-wave density-functional-theory calculations[34] of both stoichiometric and oxygen-deficient material were carried out using the plane-wave DFT code CASTEP (Ref. 35) to perform LSDA+*U* calculations.[36–40] Exchange and correlation are treated within the local spin-density approximation (LSDA) supplemented by Hubbard-*U* terms. We used Vanderbilt ultrasoft pseudopotentials,[41] retaining the O $2s^2 2p^2$ and Eu $5s^2 5p^6 6s^2 4f^7$ electrons as valence states. For calculations of bulk properties, a four-atom fcc cell was constructed while for oxygen-deficient calculations, a 64-atom simulation cell consisting of $2\times2\times2$ copies of the eight-atom cubic unit cell was constructed. A plane-wave cutoff of 600 eV was used, along with a Monkhorst-Pack[42] *k*-point grid of $4\times4\times4$ points for Brillouin-zone integrations on the 64-atom cell, and a $10\times10\times10$ grid for the two-atom cell. The basic LSDA approximation, with no onsite Hubbard-*U* terms to localize the correlated orbitals, fails to represent EuO accurately: it predicts it to be a metal with no energy gap for the majority spin channel, and predicts somewhat less than the full $7\mu_B$ per Eu atom due to the Eu $4f$ states lying at the Fermi level rather than entirely below it. The lattice parameter a_{lat} is likewise in fairly poor agreement with the experimental value of 5.14 Å (Ref. 43): an underestimate of nearly 4%. These failures are well-known to originate from the tendency of LSDA to overdelocalize the orbitals originating from atomic *f*- and *d*-like states due to spurious self-interaction of localized states.[36] We therefore employ the widely used remedy of introducing a Hubbard-*U* term to the Kohn-Sham Hamiltonian to promote integer occupation of the orbitals of the correlated subspace (in this case, the Eu $4f$ manifold). The usual approaches to determining *U* parameters are either to treat them as variable parameters and attempt to match some property of the model to an experimentally known property of the material or to calculate them from first-principles.[44] Some previous LSDA+*U* simulations of EuO (Refs. 45 and 46) have employed Hubbard-*U* terms on the $5d$ orbitals of Eu, on the basis that adjustment of both U_f and U_d simultaneously can be used to match both the energy gap and the lattice parameter simultaneously to their experimental values. However, examination of the band structure suggests that the conduction-band states originating from Eu $5d$ are strongly dispersive, as seen in Fig. 4. This suggests that the $5d$-like bands do not represent strongly localized states for which DFT+*U* is appropriate. We have tested values in the range of U_f=6.3–8.3 eV, in line with the range of previous theoretical estimates. We used linear combination of atomic orbitals states of the pseudopotential as Hubbard projectors with the spin state initialized to the ferromagnetic state in each case to aid convergence of the

TABLE IV. Oxygen-vacancy concentration and magnetic moment of EuO_{1-x}.

x_{PNR} (%)	x_M (%)	$\mu(x)$ DFT (μ_B/Eu atom)	$\mu(x)$ PNR (μ_B/Eu atom)
2.5	3.5	7.03	7.04
4.2	4.4	7.06	7.07
9	10	7.10	7.13

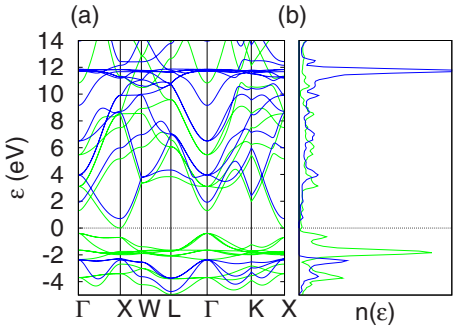

FIG. 4. (Color online) (a) Band structure and (b) density of states for bulk EuO calculated within LSDA+*U* for U_f=7.3 eV. Majority spin bands and DOS are in green (light), minority spin bands in blue (dark).

electronic energy. For each U_f value, the optimized lattice parameter and corresponding majority and minority spin energy gap were calculated. We note that variation in the specific value of U_f does not significantly affect a_{lat}, which stays constant at around 5.06Å or any other details of the geometry (atomic relaxations in the defective cells are similarly insensitive to U_f). The calculated majority spin energy gap (which is indirect between Γ in the conduction band and X in the valence band) is somewhat sensitive to U_f but for the parameters tested stayed within the range of 0.4–0.6 eV. The LSDA+U gap is therefore still considerably underestimated relative to the experimental value of 1.12 eV (Ref. 43). On the basis of this relatively small variation in the physical observables with U_f, we have chosen here an intermediate value of U_f=7.3, in line with theoretical estimates suggested elsewhere,[45–47] though of course U parameters are not directly transferable between calculations given the freedom of choices of pseudopotentials and projectors. Figures 4(a) and 4(b) show the resulting LSDA+U band structure and density of states for bulk EuO. The majority spin Eu 4f band lies well below the Fermi level, below the majority spin O 2p states while the conduction band comprises hybridized Eu 6s and 5d states. The bottom of the conduction band is seen to be spin polarized with a splitting of 0.58 eV between the majority and minority spin bands.

Oxygen-deficient cells representing EuO_{1-x} were then constructed by patterning the eight-atom cubic unit cell 2 $\times 2 \times 2$ times to form a 64-atom supercell. A proportion x of the oxygen atoms were removed from positions that ensured no pair of next-nearest-neighbor oxygens were both removed: this allows up to four of the 32 oxygens to be removed. We can thus access vacancy concentrations from x =0 to x=12.5% for this system size. Geometry relaxation of all atoms was performed. Note that due to the periodic boundary conditions imposed in DFT simulations of solids, the system studied represents a periodic array of defects rather than a random distribution. However, the change in magnetic moment per vacancy due to occupation of the conduction band would not be expected to depend strongly on the arrangement of these vacancies. Figure 5 shows the band structure and density of states of some of the resulting supercells: the effect of the vacancies is to bring down the energies of the conduction-band states on the Eu atoms adjacent to vacancy sites. Because of the aforementioned spin splitting of the conduction-band minimum, the free charge released by the creation of vacancies occupies the majority spin preferentially, enhancing the magnetic moment of the sample.

In dilute ferromagnets, the only origin of ferromagnetism is given by the exchange interaction mediated by conduction electrons,[48,49] however in EuO_{1-x} the superexchange between Eu atoms is the origin of ferromagnetic alignment, causing the spin splitting of the conduction band; the conduction-band electrons by populating the majority spin branch are ferromagnetically aligned with the 4f shells, thereby enhancing the magnetic moment. At higher vacancy concentrations, beyond those measured experimentally, the degree of polarization of the occupied conduction-band states falls due to proportionally more minority spin bands falling below the Fermi level. Table V lists the predicted moment per Eu atom for varying levels of vacancy concentration x. These results show an increasing trend with x.

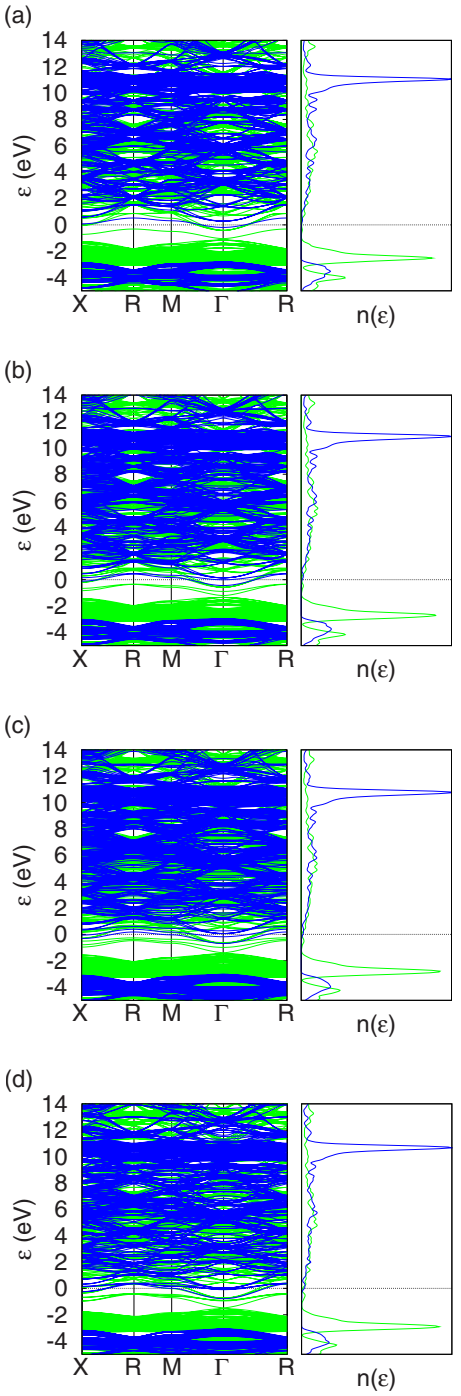

FIG. 5. (Color online) Calculated band structure and density of states, for $2 \times 2 \times 2$ supercells of EuO_{1-x}, containing (a) one vacancy (b) two vacancies (c) three vacancies and (d) four vacancies. Majority spin bands and DOS are in green (light), minority spin bands in blue (dark). Note that the energy scale is shifted relative to that in Fig. 4 and between different calculations due to differing Fermi energies. Note also the different k-point path due to the choice of a simple-cubic supercell rather than fcc.

Results corresponding to the vacancy concentrations calculated from the PNR data were interpolated to the x values sampled in the DFT calculations by using a fit to the DFT results of the form $\mu(x)=7+a_1x+a_2x^2$ μ_B/Eu atom, which

TABLE V. Oxygen-vacancy concentration x and magnetic moment of EuO_{1-x} calculated within DFT+U.

Number of vacancies/cell	x (%)	Moment per Eu atom (μ_B)
0	0.000	7.000
1	3.125	7.044
2	6.250	7.077
3	9.375	7.103
4	12.500	7.134

gives $a_1=1.37$ and $a_2=-2.53$. In Table IV we indicate the value for $\mu(x)$ thus calculated for each value of x_{PNR}.

V. MAGNETIC MOMENT OF EuO_{1-x} THIN FILMS

The electronic structure of EuO_{1-x} calculated by DFT+U indicates that the excess electrons populate preferentially the majority spin branch of the conduction band, giving rise to an enhancement of the magnetic moment per Eu atom. The moment $\mu(x)$ increases with the oxygen vacancy concentration x as shown in Tables IV and V. By comparing the predicted values of $\mu(x)$ with those measured by PNR we find a satisfactory agreement. The moment obtained from the DFT calculations and the PNR data is also plotted in Fig. 6. From this analysis we conclude that the magnetic moment of EuO_{1-x} is enhanced by the excess electrons originating from the oxygen vacancies populating the spin-polarized conduction band.

VI. SUMMARY

We have analyzed how the oxygen vacancy concentration in EuO_{1-x} influences its magnetic moment and Curie temperature. The oxygen vacancy concentration in EuO_{1-x} acts as a dopant and thereby controls the conduction-band electron concentration. We were able to measure precisely the oxygen vacancy concentration by independently fitting PNR data and Curie temperature measurements made by SQUID and fitted with a model developed by Mauger.[7,27] It has been shown previously that these excess electrons populate preferentially the majority spin branch of the conduction band at lower concentrations and can modulate the conductivity of EuO_{1-x} and match it with that of Si.[3,4] We found by PNR measurements that the magnetic moment is enhanced with the oxygen vacancy concentration. By studying the electronic structure of EuO_{1-x} through DFT+U theory calculations, we have determined quantitatively the expected enhancement of the magnetic moment caused by the excess electrons and found it to be in good agreement with our experimental results. These electrons mediate an additional ferromagnetic exchange interaction which increases the magnetic moment. The degree of polarization of the conduction band decreases at higher concentrations, when the minority spin branch is progressively lowered below the Fermi level.

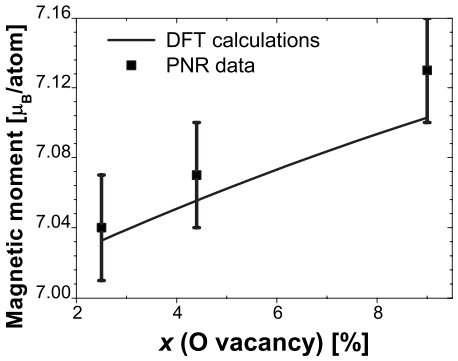

FIG. 6. Magnetic moment of oxygen-deficient EuO as a function of the oxygen vacancy concentration as calculated by DFT and measured by PNR at 5 K.

ACKNOWLEDGMENTS

We would like to thank K. Ziebeck for his contributions and ISIS for funding the PNR measurements.

*massimokriya@gmail.com
†chwb101@cam.ac.uk

[1] D. P. DiVincenzo, J. Appl. Phys. **85**, 4785 (1999).
[2] D. Loss and D. P. DiVincenzo, Phys. Rev. A **57**, 120 (1998).
[3] A. Schmehl, V. Vaithyanathan, A. Herrnberger, S. Thiel, C. Richter, M. Liberati, T. Heeg, M. Röckerath, L. Fitting Kourkoutis, S. Mühlbauer, P. Böni, D. A. Muller, Y. Barash, J. Schubert, Y. Idzerda, J. Mannhart, and D. G. Schlom, Nature Mater. **6**, 882 (2007).
[4] R. P. Panguluri, T. S. Santos, E. Negusse, J. Dvorak, Y. Idzerda, J. S. Moodera, and B. Nadgorny, Phys. Rev. B **78**, 125307 (2008).
[5] P. Sinjukow and W. Nolting, Phys. Rev. B **68**, 125107 (2003).
[6] E. L. Nagaev, *Physics of Magnetic Semiconductors* (Mir, Moscow, 1983).
[7] A. Mauger and C. Godart, Phys. Rep. **141**, 51 (1986).
[8] P. G. Steeneken, Ph.D. thesis, University of Groningen, 2002.
[9] P. G. Steeneken, L. H. Tjeng, I. Elfimov, G. A. Sawatzky, G. Ghiringhelli, N. B. Brookes, and D. J. Huang, Phys. Rev. Lett. **88**, 047201 (2002).
[10] T. S. Santos, J. S. Moodera, K. V. Raman, E. Negusse, J. Holroyd, J. Dvorak, M. Liberati, Y. U. Idzerda, and E. Arenholz, Phys. Rev. Lett. **101**, 147201 (2008).
[11] T. S. Santos and J. S. Moodera, Phys. Rev. B **69**, 241203(R) (2004).
[12] A. Mauger, C. Godart, M. Escorne, J. C. Achard, and J. P. Desfours, J. Phys. (Paris) **39**, 1125 (1978).
[13] A. Mauger, M. Escorne, C. Godart, J. P. Desfours, and J. C. Achard, J. Phys. (Paris), Colloq. **41**, C5-263 (1980).
[14] T. J. Konno, N. Ogawa, K. Wakoh, K. Sumiyama, and K. Su-

zuki, Jpn. J. Appl. Phys., Part 1 **35**, 6052 (1996).
[15] A. A. Samokhvalov, A. F. Gunichev, B. A. Gizhevskii, N. N. Loshkareva, N. M. Chebotaev, and N. A. Viglin, Sov. Phys. Solid State **20**, 519 (1978).
[16] O. Massenet, Y. Capiomont, and N. Van Dang, J. Appl. Phys. **45**, 3593 (1974).
[17] T. Matsumoto, K. Yamaguchi, M. Yuri, K. Kawaguchi, N. Koshizaki, and K. Yamada, J. Phys.: Condens. Matter **16**, 6017 (2004).
[18] Y. Shapira, S. Foner, and T. B. Reed, Phys. Rev. B **8**, 2299 (1973).
[19] A. Mauger, Phys. Status Solidi B **84**, 761 (1977).
[20] G. P. Felcher, J. Appl. Phys. **87**, 5431 (2000).
[21] J. A. C. Bland and C. A. F. Vaz, in *Ultrathin Magnetic Structures*, edited by J. A. C. Bland and B. Heinrich (Springer, New York, 2005).
[22] R. Felici, J. Penfold, R. C. Ward, and W. G. Williams, Appl. Phys. A: Mater. Sci. Process. **45**, 169 (1988).
[23] S. J. Blundell and J. A. C. Bland, Phys. Rev. B **46**, 3391 (1992).
[24] http://www.isis.stfc.ac.uk
[25] Data fitted with XPOLLY available on the CRISP website.
[26] M. Arnold and J. Kroha, Phys. Rev. Lett. **100**, 046404 (2008).
[27] H. Ott, S. J. Heise, R. Sutarto, Z. Hu, C. F. Chang, H. H. Hsieh, H. J. Lin, C. T. Chen, and L. H. Tjeng, Phys. Rev. B **73**, 094407 (2006).
[28] A. S. Borukhovich, V. G. Bamburov, and A. A. Sidorov, J. Magn. Magn. Mater. **73**, 106 (1988).
[29] A. Mauger and P. Leroux Hugon, Physica B **86-88**, 1007 (1977).
[30] Scattering lengths taken from the NIST website http://www.ncnr.nist.gov/resources/n lengths/
[31] R. W. Ulbricht, A. Schmehl, T. Heeg, J. Schubert, and D. G. Schlom, Appl. Phys. Lett. **93**, 102105 (2008).
[32] J. Lettieri, V. Vaithyanathan, S. K. Eah, J. Stephens, V. Sih, D. D. Awschalom, J. Levy, and D. G. Schlom, Appl. Phys. Lett. **83**, 975 (2003).
[33] A. Comment, J.-P. Ansermet, C. P. Slichter, H. Rho, C. S. Snow, and S. L. Cooper, Phys. Rev. B **72**, 014428 (2005).
[34] M. C. Payne, M. P. Teter, D. C. Allan, T. A. Arias, and J. D. Joannopoulos, Rev. Mod. Phys. **64**, 1045 (1992).
[35] S. J. Clark, M. D. Segall, C. J. Pickard, P. J. Hasnip, M. J. Probert, K. Refson, and M. C. Payne, Z. Kristallogr. **220**, 567 (2005).
[36] V. I. Anisimov, J. Zaanen, and O. K. Andersen, Phys. Rev. B **44**, 943 (1991).
[37] V. I. Anisimov and O. Gunnarsson, Phys. Rev. B **43**, 7570 (1991).
[38] V. I. Anisimov, F. Aryasetiawan, and A. I. Liechtenstein, J. Phys.: Condens. Matter **9**, 767 (1997).
[39] A. I. Liechtenstein, V. I. Anisimov, and J. Zaanen, Phys. Rev. B **52**, R5467 (1995).
[40] S. L. Dudarev, G. A. Botton, S. Y. Savrasov, C. J. Humphreys, and A. P. Sutton, Phys. Rev. B **57**, 1505 (1998).
[41] D. Vanderbilt, Phys. Rev. B **41**, 7892 (1990).
[42] H. J. Monkhorst and J. D. Pack, Phys. Rev. B **13**, 5188 (1976).
[43] P. Wachter, in *Handbook on the Physics and Chemistry of Rare Earths*, edited by K. A. Gschneidner and L. Eyring (Elsevier, Amsterdam, 1979), Vol. 2.
[44] M. Cococcioni and S. de Gironcoli, Phys. Rev. B **71**, 035105 (2005).
[45] D. B. Ghosh, M. De, and S. K. De, Phys. Rev. B **70**, 115211 (2004).
[46] P. Larson and W. R. L. Lambrecht, J. Phys.: Condens. Matter **18**, 11333 (2006).
[47] N. J. C. Ingle and I. S. Elfimov, Phys. Rev. B **77**, 121202 (2008).
[48] C. Zener, Phys. Rev. **81**, 440 (1951).
[49] T. Dietl, H. Ohno, F. Matsukura, J. Cibert, and D. Ferrand, Science **287**, 1019 (2000).